nature genetics

Lamin B1 duplications cause autosomal dominant leukodystrophy

Quasar S Padiath[1], Kazumasa Saigoh[1,8], Raphael Schiffmann[2], Hideaki Asahara[3], Takeshi Yamada[4], Anulf Koeppen[5], Kirk Hogan[6], Louis J Ptáček[1,7] & Ying-Hui Fu[1]

Adult-onset autosomal dominant leukodystrophy (ADLD) is a slowly progressive neurological disorder characterized by symmetrical widespread myelin loss in the central nervous system, with a phenotype similar to chronic progressive multiple sclerosis. In this study, we identify a genomic duplication that causes ADLD. Affected individuals carry an extra copy of the gene for the nuclear laminar protein lamin B1, resulting in increased gene dosage in brain tissue from individuals with ADLD. Increased expression of lamin B1 in *Drosophila melanogaster* resulted in a degenerative phenotype. In addition, an abnormal nuclear morphology was apparent when cultured cells overexpressed this protein. This is the first human disease attributable to mutations in the gene encoding lamin B1. Antibodies to lamin B are found in individuals with autoimmune diseases, and it is also an antigen recognized by a monoclonal antibody raised against plaques from brains of individuals with multiple sclerosis. This raises the possibility that lamin B may be a link to the autoimmune attack that occurs in multiple sclerosis.

Hereditary leukodystrophies are rare disorders in which the loss of myelin is a primary condition rather than secondary to neuronal degeneration. In these disorders, variable degrees of demyelination occur in either the central nervous system (CNS), the peripheral nervous system or both[1]. Adult-onset autosomal dominant leukodystrophy (ADLD) was first described in an Irish-American family[2]. It is slowly progressive and fatal, presenting in the fourth or fifth decade of life, characterized clinically by early autonomic abnormalities, pyramidal and cerebellar dysfunction and symmetrical demyelination of the CNS[3]. These individuals are frequently diagnosed as having chronic progressive multiple sclerosis[2]. However, ADLD differs from multiple sclerosis and other demyelinating disorders in that neuropathology shows preservation of oligodendroglia in the presence of subtotal demyelination and lack of astrogliosis[4]. Most hereditary leukodystrophies are either autosomal recessive or X-linked recessive, and the age of onset is typically during infancy or childhood (as in the cases of Krabbe globoid cell leukodystrophy, Pelizaeus-Merzbacher disease (PMD) and adrenoleukodystrophy)[1]. In contrast, ADLD is a highly penetrant, autosomal dominant, adult-onset disorder that we had previously mapped to chromosome 5q (ref. 4).

We now report identification of a tandem genomic duplication, which results in an extra copy of the gene encoding the nuclear lamina protein lamin B1 (*LMNB1*), that causes ADLD. We found duplications of the *LMNB1*-containing region in the original and in three other families with similar clinical and magnetic resonance imaging (MRI) features. The duplication resulted in increased gene dosage of *LMNB1* in brain tissue from affected individuals. Overexpression of *LMNB1* in *Drosophila melanogaster* and in a cell culture system resulted in a degenerative phenotype and abnormal nuclear morphology, respectively. ADLD is the first disease recognized to result from *LMNB1* mutations and suggests a previously unknown role for the involvement of the nuclear envelope in disorders of the CNS.

RESULTS

Linkage analysis and mutation screening

We identified an additional kindred, K4233, with clinical features similar to that of the original ADLD kindred K2685 (ref. 4) (**Fig. 1**). Linkage analysis showed that the disease gene mapped to the same chromosomal region as K2685, and by analyzing individuals in which recombination had occurred in both families, we narrowed the critical region containing the disease gene to a 4-Mb region on chromosome 5q between markers D5S2059 and D5S1841 (data not shown). As both families were of Irish-American descent, and given the rarity of the disease, we hypothesized that the disease in both families arose from a common founder mutation. During the course of the study, we also obtained DNA from two other families, K4975 and K50069 (**Fig. 1**), with similar clinical and MRI features[5] (data not shown).

[1]Department of Neurology, University of California, San Francisco, San Francisco, California, USA 94158. [2]Developmental and Metabolic Neurology Branch, National Institute of Neurological Disorders and Stroke, US National Institutes of Health, Bethesda, Maryland 20892, USA. [3]Department of Neurology, Faculty of Medicine, Kyushu University, Kyushu, Japan. [4]Department of Neurology, Iizuka Hospital, Iizuka City, Japan. [5]Veterans Administration Medical Center and Department of Neurology, Albany Medical College, Albany 12208, New York, USA. [6]Department of Anesthesiology, University of Wisconsin, Madison, Wisconsin 53792, USA. [7]Howard Hughes Medical Institute, San Francisco, California 94158, USA. [8]Present address: Department of Neurology, Kinki University School of Medicine, Osaka, Japan. Correspondence should be addressed to Y.-H.F. (yhf@neugenes.org).

Received 12 May; accepted 31 July; published online 3 September; corrected 12 September 2006; corrected after print 22 January 2007; doi:10.1038/ng1872

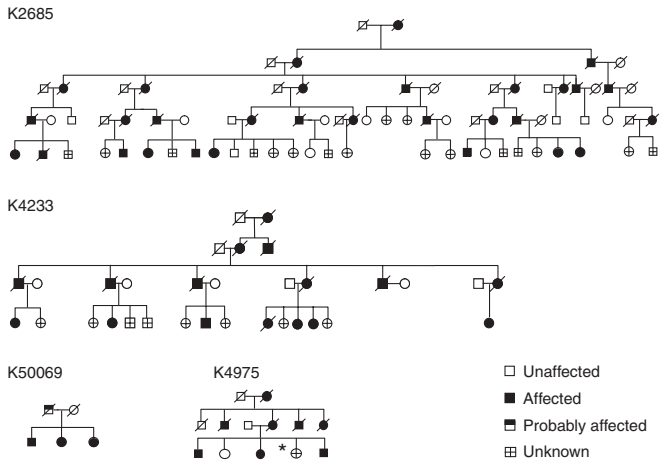

Figure 1 Pedigree charts of ADLD families. See Results section for details on analysis of genomic copy number variation.

To identify disease-causing mutations, we sequenced exons of all known genes and mRNA species in the critical region in affected individuals from K2685 and K4233 (**Supplementary Table 1** online). We sequenced genomic DNA from affected individuals and also from mouse-human hybrid cell lines derived from cells of affected individuals. The hybrid cell lines enabled us to separate chromosomes derived from each of the two parents of an individual and to assign phase unambiguously when identifying sequencing variants. We constructed a haplotype map of the chromosome on which the disease-causing mutation lies (the disease chromosome) from both pedigrees and observed a large shared haplotype block in the critical region, further suggesting that both families arose from a common founder (**Fig. 2a**). Sequencing the genes in the region did not uncover any disease-specific mutations.

Identification of a duplicated genomic segment

During sequencing, we noticed the presence of a double peak at SNP locus rs4331946 in the hybrid cell line samples derived from the disease chromosome from an affected individual in K4233 (**Fig. 2b,c**). As the hybrid cell lines are haploid for the ADLD locus, a sequencing peak corresponding to only one of the alleles is expected. The extra peak suggested the presence of a duplication that was recognized because there was a single–base pair difference between the two copies. This double peak was present only in the cell line derived from the disease chromosome of the affected individual from K4233 and not from the normal chromosome or from the cell lines derived from affected individuals in K2685 (**Fig. 2c**). We also observed this pattern in other SNP loci: notably, only SNPs that were telomeric to rs4331946 (up to ~50 kb) in the hybrid cell line derived from the K4233 individual showed double peaks. We did not see this pattern in SNP loci centromeric to rs4331946 or in hybrid cell lines derived from the normal chromosome or those derived from affected individuals from K2685. The locations of SNP loci demonstrating this peak pattern were in the non-shared region just beyond the telomeric boundary of the shared haplotype block (**Fig. 2b**). The peak pattern was specific to this chromosomal region, as other informative loci in regions at distances greater than 100 kb on either side of rs4331946 did not show the heterozygous peak pattern in any of the hybrid cell lines sequenced.

We next sequenced this region of genomic DNA from affected individuals from whom the cell lines were derived. The peak height ratios of the alleles showed a consistent difference between affected individuals and controls (**Fig. 2c**). In affected individuals from K2685, the ratio of peak height of the allele from the disease chromosome (D) relative to that from the normal chromosome (N) was always higher than in normal controls. In affected individuals from K4233, a similar pattern was observed in the SNP loci that were centromeric to rs4331946. This could be explained if we assumed that the duplication was intrachromosomal. Therefore, the haplotype of the original and duplicated sequence would be the same: that is, the original and duplicated sequence would share the same SNP alleles. Thus, the disease chromosome would contribute two copies of one allele (because it is a duplication), and the normal chromosome would contribute one copy of the second allele, resulting in a higher relative peak height of the alleles from the disease chromosome (D:N, 2:1) (**Fig. 2d**). However, in the SNP loci that were telomeric to rs4331946 in K4233, we observed that the peak height ratios of the alleles from the normal chromosome were relatively higher than when compared with normal individuals (N:D, 2:1). We also identified microsatellite markers in the duplicated region that had three alleles in affected individuals from K4233 (**Fig. 2b,e**). These data could be explained if we assume that the duplication occurred in a tandem orientation and that a recombination event occurred at some point after the duplication (**Fig. 2f**). If the recombination involved part of the chromosomal region that was duplicated, this would result in part of the duplicated region having a haplotype of the recombined homologous chromosome which would be different from that of the original sequence from which it was duplicated. The boundary of the shared haplotype block would mark the site of the recombination event, and this would explain the presence of the double peaks in the haploid hybrid cell line DNA and the occurrence of three alleles in the microsatellite loci only in SNP loci that were within the duplicated region and telomeric to the shared haplotype block (that is, in the non-shared region).

Analysis of genomic copy number variation

To independently confirm this genomic copy number variation, we used two different approaches: DNA blotting and real-time quantitative PCR analysis using TaqMan probes. For DNA blotting, we hybridized genomic DNA from affected individuals and controls with a probe from within the region we thought to be duplicated. The samples from affected individuals showed a relative increase in normalized intensity of the band from the putative duplicated region in comparison with control individuals (**Fig. 3a**). Quantitation of the band's relative intensity revealed an increase of ~1.4- to 1.8-fold over normal controls (**Fig. 3b**). This is similar to an expected ratio of 1.5 if there were one extra copy of the genomic sequence, as affected individuals would have three copies of this region, and normal individuals would have two copies.

TaqMan quantitative PCR analysis is an extremely sensitive method for the study of copy number variations and has been used in the detection of other diseases such as Charcot-Marie-Tooth type 1A, caused by genomic duplications[6]. Using this assay with primers from exon 4 of the gene, *LMNB1*, which is within the putative duplication region, we found that affected individuals from K2685, K4233, K4975 and K50069 had a mean copy number of 1.7 (range = 1.4–2.0, $n = 15$, s.d. = 0.16), compared with normal controls, who had a mean copy number of 0.89 (range = 0.6–1.16, $n = 108$, s.d. = 0.11) (**Fig. 3c**). The fact that the duplication was not present in 108 normal controls confirmed that it was not a normal polymorphism. The duplication was also present in one individual from K4975 diagnosed as unknown at the time of DNA isolation (marked by * in K4975, **Fig. 1**).

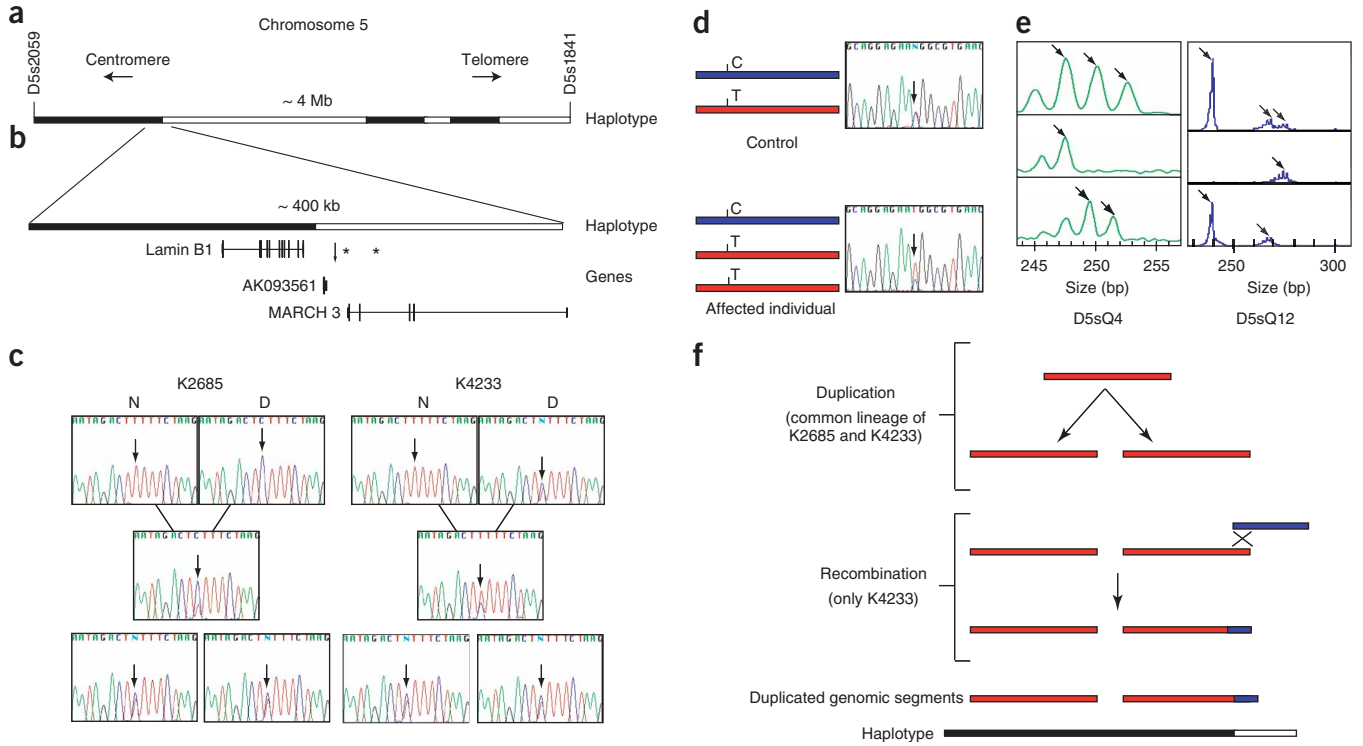

Figure 2 Identification of a duplicated genomic segment within the critical region. (**a**) Haplotype analysis in K2685 and K4233 (not drawn to scale). Filled bars represent shared haplotypes, and open bars represent non-shared haplotypes. (**b**) A high-resolution map of the proximal shared haplotype boundary. The arrow shows the approximate location of the SNP locus rs4331946. * marks the two microsatellite loci that showed three peaks in the affected individuals from K4233. (**c**) Sequencing of the SNP locus rs4331946. Top row: hybrid cell line DNA (N, normal; D, diseased). Center row: genomic DNA. Bottom row: genomic DNA, normal controls. (**d**) A schematic representation of how the altered peak height ratio might arise at SNP loci owing to a duplication. (**e**) Microsatellite loci D5SQ4 and D5SQ12 showing three peaks in affected individuals from K4233. The positions of these loci are indicated by * in **b**. These microsatellite markers lie just beyond the shared haplotype boundary in the critical region but are still part of the duplication (the blue segment of the duplicated region in **f**). Upper boxes: genomic DNA of affected individual from K4233. Center boxes: hybrid cell line DNA of normal chromosome. Lower boxes: hybrid cell line DNA of disease chromosome. Arrows point to allele peaks. (**f**) A schematic representation of the possible sequence of events explaining the presence of the double peak in DNA in hybrid cell lines derived from affected individuals in K4233 and the three peaks in microsatellite markers in a portion of the duplicated segment.

As she was younger than her affected siblings, it is likely that she may develop the disease at a later age[5].

Identification of duplication sizes, junctions and locations

We used the relative peak height ratio differences as an index to identify the extent of the duplication. Using this technique, we typed informative SNP loci on either side of the originally identified duplication, moving outward until we reached loci where the peak height ratio was the same between affected individuals and controls (**Fig. 4a**). These loci marked the centromeric and telomeric boundaries of the duplication. The boundaries were further refined using more closely spaced SNPs until duplicated SNPs were separated from nonduplicated SNPs by only a few kilobases. Using this method in affected individuals from families K4233 and K2685, we were able to identify the duplication junction to a resolution of ~3 kb on the centromeric end (**Fig. 4a**). We further resolved the position of the duplication junction by carrying out long PCR reactions (**Fig. 4b**,**c**). We used a forward primer on one side of the duplicated SNP and reverse primers at successively longer distances away from the SNP and used peak height ratio as the readout (**Fig. 4c**). The first primer combination that produced a peak height ratio readout similar to that of controls marked the nonduplicated boundary. Thus, we were able to narrow the centromeric end of the duplicated region to ~180 bp (**Fig. 4c**). We then performed inverse PCR to identify the exact duplication junction sequence and thereby identify the location of the duplicated genomic segment and its size. Sequencing the inverse PCR products showed that the duplication was arranged in a head-to-tail tandem orientation (**Fig. 5a**). The duplication junction was identical for affected individuals from K2685 and K4233, confirming that the mutations arose from a common founder. The size of the duplication was 169,455 bp (**Fig. 5b**), and the segment that was duplicated lay between 126124775 (± 2) and 126294230 (± 2) bp.

We used a similar approach to determine that the duplication in K50069 was 340,785 bp and that the duplicated segment lay between 126031182 (± 2) and 126371967 (± 2) bp. For the K4975 kindred, we mapped the centromeric and telomeric junctions to within ~31 kb and ~69 kb, respectively, and demonstrated that they were different from both K2685 and K50069. The fact that the duplication breakpoints were unique to each of the three families proved that they represented independent mutational events (**Fig. 5b**).

We also designed primers that spanned the putative duplication junction sequences for both characterized duplications (T1-C2 in **Fig. 5a**). These primer sets produced an amplification product specific and unique to affected individuals in each family. We used PCR at the duplication junctions to confirm that the duplication cosegregated

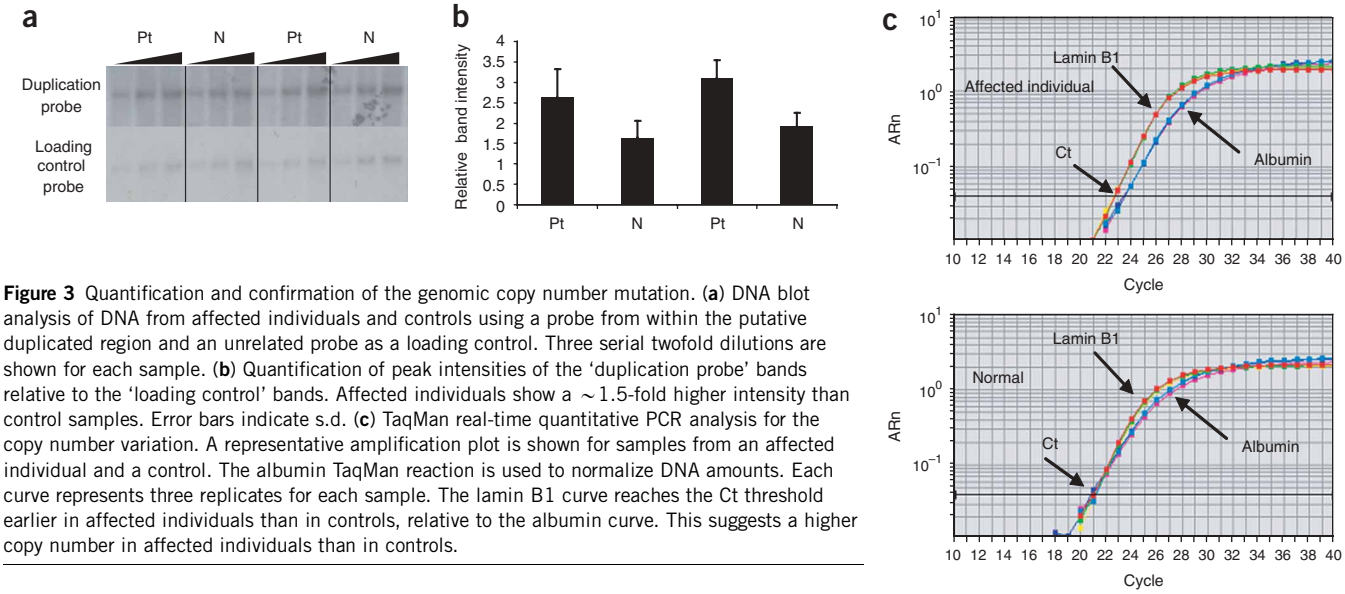

Figure 3 Quantification and confirmation of the genomic copy number mutation. (**a**) DNA blot analysis of DNA from affected individuals and controls using a probe from within the putative duplicated region and an unrelated probe as a loading control. Three serial twofold dilutions are shown for each sample. (**b**) Quantification of peak intensities of the 'duplication probe' bands relative to the 'loading control' bands. Affected individuals show a ~1.5-fold higher intensity than control samples. Error bars indicate s.d. (**c**) TaqMan real-time quantitative PCR analysis for the copy number variation. A representative amplification plot is shown for samples from an affected individual and a control. The albumin TaqMan reaction is used to normalize DNA amounts. Each curve represents three replicates for each sample. The lamin B1 curve reaches the Ct threshold earlier in affected individuals than in controls, relative to the albumin curve. This suggests a higher copy number in affected individuals than in controls.

with the disease phenotype in kindreds 2685, 4233, and 50069. We performed this junction PCR in ~200 normal controls and did not find any amplification products in these samples.

Analysis of the duplication junction sequences

We analyzed the duplication junction sequences (T1-C2) in K2685 and K50069 to look for sequence motifs potentially mediating the duplication events (**Fig. 5c**). We did not find any significant sequence identity between the telomeric (T1) and centromeric (C2) ends up to 100 bp on either side of the duplication, and these sequences matched the reference sequence perfectly. At both the T1 and C2 ends, in both families, there was a sequence identity of 2 bp. (**Fig. 5c**). A region of microhomology is one of the features observed as a result of junctions formed by a nonhomologous end-joining repair process[7–11]. The sequence at both ends of the duplicated segment (N1-C1 and T2-N2; **Fig. 5a**) matched the reference sequence perfectly with no deletions or insertions. The sequences at the centromeric ends (N1-C1) in both families (K2685 and K50069) were in a region rich in Alu repeats. An AluY repeat ~60 bp from the N1-C1 junction in K2685 affected individuals showed 79% identity to an AluJb repeat ~600 bp from the N1-C1 junction region in K50069. Homopolymeric stretches of A or T nucleotides were found around the N1-C1 end in the two families studied. In the case of K50069, the duplication junction at the centromeric end fell within a simple tandem repeat with a consensus sequence of ACAAAGTACCTTCTTAAGGGTGGGG GAGAATATT that repeated 10.7 times. We were unable to identify any low-complexity repeats in a 2-Mb sequence around the duplication region, suggesting that nonallelic homologous recombination[12] is unlikely to have a role in these duplications (data not shown). Taken together, the data suggest that ADLD duplications may have arisen as a result of coupled homologous and nonhomologous recombination completed by nonhomologous end joining similar to that postulated for Pelizaeus-Merzbacher disease duplications[7,8,13].

LMNB1 is a candidate gene within the duplicated region

The duplicated region in all kindreds fully encompasses two known protein-coding genes, *LMNB1* and *AK093561* (**Fig. 5a**). *LMNB1* is a well-studied gene that encodes a component of the nuclear lamina that is widely expressed[14,15]. *AK093561* encodes a 241–amino acid protein of unknown function (University of California Santa Cruz (UCSC) genome browser (http://www.genome.ucsc.edu/), May 2004). Using RT-PCR analysis, we determined that *AK093561* was not expressed in the brain (data not shown) and thus is unlikely to contribute to the ADLD phenotype. The genomic rearrangement also results in a partial duplication of another gene, *MARCH3*, that is expressed in the brain (data not shown). The first exon of this gene, which includes part of the 5′ UTR, is not part of the duplicated segment in K4233 and K2685, and in K4974 only the terminal two of the five exons are duplicated (**Fig. 5a**). This makes it unlikely that the partially duplicated copy of the gene is functional, as it is probably not transcribed. RNA blot analysis using RNA from brain tissue of affected individual and controls showed no differences between the two samples when a *MARCH3*-specific probe was used (data not shown).

As the duplicated region did not result in the disruption of any known genes, we hypothesized that the disease phenotype might be caused by an increase in gene dosage. The most obvious candidate was *LMNB1*, as it was the only gene expressed in brain that was duplicated in its entirety in all families. The duplications, in all the cases, include at least 16 kb of sequence upstream from the transcription start site of *LMNB1*. Previous studies have shown that a 2-kb region upstream of the transcription initiation site is sufficient for its expression[16]. Thus, the duplicated copy is likely to contain all the promoter elements required for normal expression of the gene.

Lamin B1 is overexpressed in brain tissue of affected individuals

Analysis of RNA from different regions of the brain from a normal control showed similar expression levels of *LMNB1*, except in the cerebellum, which showed much higher expression (**Fig. 6a**). We analyzed levels of *LMNB1* expression in tissues from affected individuals relative to normal controls using RNA blotting, TaqMan PCR analysis of cDNA, and protein blot analysis (**Fig. 6b,c** and **Supplementary Table 2** online). In all the assays, there was a marked increase in expression levels in individual 1 and more modest increases in individuals 2 and 3 relative to control samples. This suggested that the duplication resulted in increased *LMNB1* gene dosage. It is unclear as to why individual 1 showed such a marked increase in *LMNB1* expression.

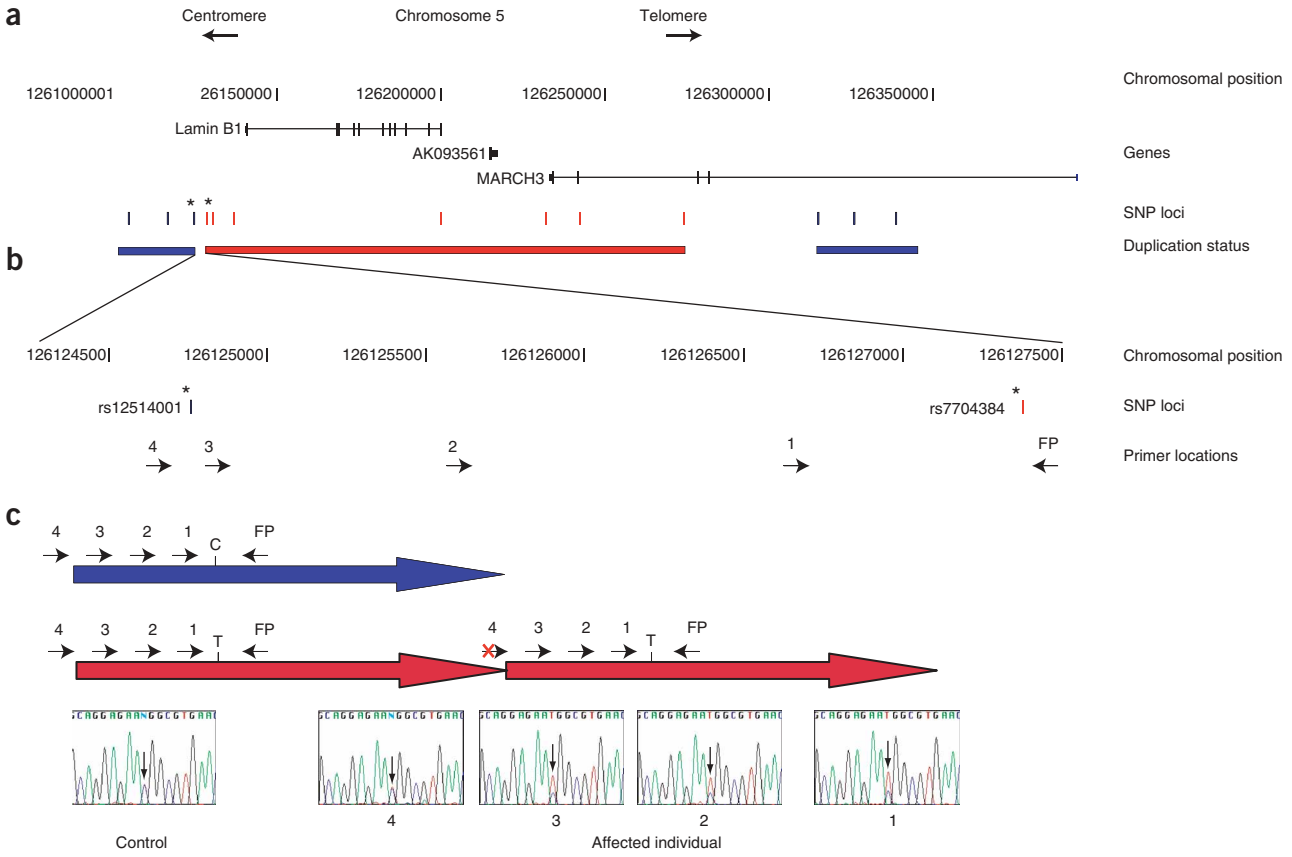

Figure 4 Mapping duplication junctions in affected individuals using the allele peak height ratio assay. (**a**) Mapping of the duplication junction in affected individuals from K2685. Informative SNP loci that showed altered peak height ratios when compared with normal controls (and assumed to be duplicated) are shown in red. Informative loci that show peak height ratios similar to normal controls are shown in blue. The SNP loci marking the centromeric boundaries of the duplication junction are marked by asterisks. (**b**) The boundaries of the duplication junction were further narrowed using a long PCR assay. Arrows indicate the locations of primers. (**c**) A schematic representation showing peak height ratios when different primer sets are used. Primers 1, 2 and 3 bind to both copies of the duplicated sequence, whereas primer 4 binds to only one copy. As a result, the sequence of the PCR product generated by primer 4 shows a peak height ratio similar to that of control samples, whereas other primers showed an altered peak height. Thus, the duplication junction must lie between primers 3 and 4. FP, forward primer.

Lamin B1 overexpression in *D. melanogaster*

We used the fruit fly *D. melanogaster* to study the *in vivo* effects of *LMNB1* overexpression. The gene encoding the principal lamin in *D. melanogaster* (*lamin* Dm_0) has 39% sequence identity to the human *LMNB1*. We generated transgenic flies expressing either the human or fly *LMNB1* orthologs in different tissues using the GAL4-UAS transformation system[17]. Ectopic expression of human disease genes in the *D. melanogaster* eye has been established as a powerful system to study the deleterious effects of these genes[18]. Targeted expression of either of the *LMNB1* orthologs in the developing eye using an eye-specific promoter, *gmr-GAL4* (ref. 19), resulted in disrupted eye morphology, loss of pigmentation and in some cases, lethality (**Fig. 7a**, upper row). We tested four lines for the *lamin* Dm_0 transgene. In two of the fly lines that strongly expressed the *lamin* Dm_0 gene under the *gmr-GAL4* promoter, there was a high degree of lethality. The few adult flies that did emerge showed severely deformed eyes that were smaller in size, with an almost complete lack of pigmentation and normal ommatidia (**Fig. 7a**, upper left). The two fly lines moderately expressing the transgene showed marked roughening and slight reduction in eye size accompanied by a patchy and irregular pigment loss (**Fig. 7a**, upper row, center).

Only one of the four fly lines transgenic for human *LMNB1* gene (**Fig. 7a**, upper right) showed a phenotype characterized by pigment loss, a reduction in eye size and moderate roughening, which was much less severe when compared with the overexpression of the fly *lamin* Dm_0. Only at 29 °C (a temperature at which *GAL4* expression is increased) did the other three lines show a slight but distinct roughening of eyes without appreciable loss of pigmentation. It is unclear whether the difference in severity results from a qualitative difference between the human and fly lamins or if it is simply because of reduced expression from the human lamin transgenic fly lines.

Expression of *lamin* Dm_0, the fly ortholog, using *elav-GAL4* and *repo-GAL4* drivers, which drive expression in neuronal and glial tissues[20,21], respectively, resulted in complete lethality in all four lines tested. Flies transgenic for human *LMNB1* showed varying degrees of lethality in the four lines studied. Notably, the expression of the fly *lamin* Dm_0 gene resulted in complete lethality at 25 °C using a more restrictive glial driver, *SPG-GAL4* in all four lines. This driver targets gene expression in a very specific subset of glial cells involved in ensheathment and insulation of the nervous system[22].

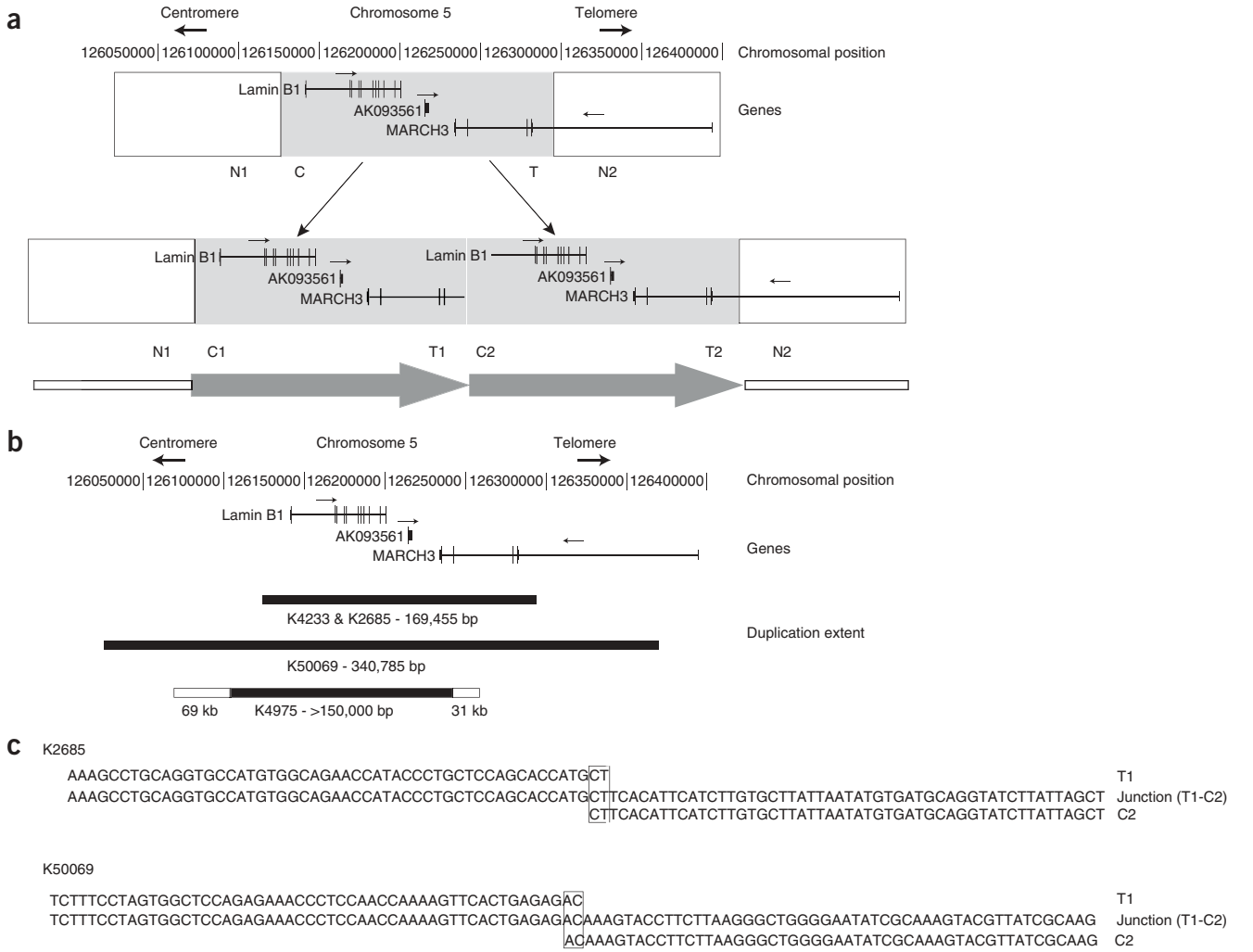

Figure 5 Schematic representation showing genomic structure of the duplications. (**a**) The genes *LMNB1* and *AK093561* are completely duplicated. Note that *MARCH3* is only partially duplicated. Arrows above the genes represent the direction of transcription. The different junction boundaries are marked. T1-C2 is the unique junction sequence seen only in affected individuals. (**b**) The size and extent of the duplication is shown for the different families. Arrows above the genes represent the direction of transcription. (**c**) Junction sequences at the T1-C2 boundary. Note that there is a sequence identity of 2 bp at the T1 and C2 junctions (boxed sequences).

Lamin B1 overexpression in cell culture

We also examined the effects of lamin B1 overexpression at the cellular level. We transfected a *LMNB1*-GFP construct into HEK293 (**Fig. 7b**) and HeLa (data not shown) cell lines and examined them after 1 d. Cells that expressed relatively low levels of *LMNB1*, as visualized by GFP fluorescence, did not show any alteration in nuclear or cellular morphology, and the LMNB1-GFP was localized to the nuclear membrane (**Fig. 7b**, lower row). Cells that expressed high levels of LMNB1-GFP, as visualized by GFP fluorescence, showed a marked increase in the surface area of the nuclear envelope accompanied by extensive folding and blebbing of the nuclear membrane (**Fig. 7b**, upper row). A similar phenotype has been reported previously with overexpression of *LMNB1* in mouse C2C12 cell lines[23].

DISCUSSION

A number of reasons make *LMNB1* an attractive candidate gene for the ADLD disease pathology, although it is still possible that other unidentified transcripts or genomic elements within the duplicated segment may also be involved. *LMNB1* is the only reported gene within the duplicated region that is expressed in the brain. The lamin B1 protein is a member of the intermediate filament family of proteins and is part of the nuclear lamina that underlies the nuclear envelope of eukaryotic cells[14]. Mutations in another intermediate filament protein, glial fibrillary acidic protein (GFAP), have been implicated in Alexander disease, a childhood onset demyelinating disorder[24]. Vertebrate lamins are classified into two types, A and B. Mammalian somatic cells show two major species of each type: lamins A/C for the A type (alternate splice variants of the same gene) and B1 and B2 (coded for by independent genes) for the B type[14]. Mutations in gene encoding lamins A/C are responsible for a wide range of diseases, including Charcot-Marie-Tooth neuropathy type 2 B1 (CMT2B1) which is characterized by peripheral loss of large myelinated fibers and axonal degeneration[25–27]. Mutations in emerin, another nuclear membrane protein, are responsible for Emery-Dreifuss-type muscular dystrophy, which is also caused by mutations in the genes encoding lamins A/C[28,29]. Although mutations in the gene encoding lamins A/C have

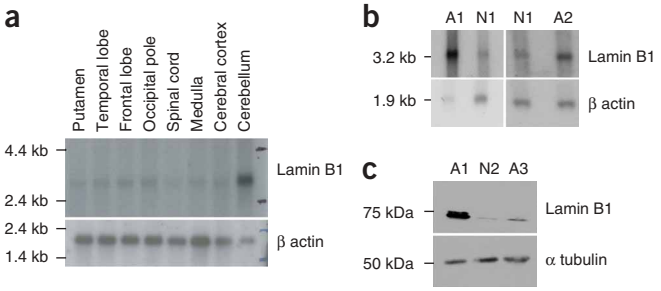

Figure 6 Lamin B1 shows increased expression in brain tissue from affected individuals. (**a**) RNA blot analysis of *LMNB1* expression in different regions of the CNS from a normal control. We used 2 μg of mRNA from each region. (**b**) RNA blot analysis of mRNA samples from brain tissue from controls and affected individuals. (**c**) Protein blot analysis of protein lysate from brain tissue from controls and affected individuals. N1 and N2 are the two control individuals from whom tissue samples were obtained and A1, A2 and A3 are the three affected individuals from whom tissue samples were obtained. All the affected individuals were from the K2685 kindred.

been shown to result in at least nine distinct disorders[27], ADLD is the first human disease attributed to mutations of lamin B1. Recently, mutations in lamin B2 were shown to be associated with acquired partial lipodystrophy[30].

Previous studies have shown that overexpression of both wild-type lamin B1 and lamins A and C result in an abnormal nuclear morphology[23]. This suggests that maintaining stoichiometric amounts of these proteins might be important for proper assembly of the nuclear membrane. Altering relative amounts of the laminar proteins thus may affect the structural integrity of the nuclear membrane and produce cellular dysfunction. Notably, other central and peripheral demyelinating disorders such as Pelizaeus-Merzbacher disease and Charcot-Marie-Tooth neuropathy type 1A can also be caused by duplications, suggesting that the cellular processes that are involved in myelin formation might be uniquely susceptible to gene dosage[13,31]. *LMNB1* overexpression may also produce a disease phenotype by modulating gene expression, as the nuclear lamina is known to have a role in chromatin organization and transcriptional regulation[14,26,32].

ADLD is one of the few adult onset demyelinating disorders[1]. It might also be possible that the accumulation of the lamin B1 protein is toxic over time to certain cell types, thereby producing the phenotype at a later age. Recent studies have suggested that nuclear architecture undergoes progressive age-related changes, in part influenced by levels of lamin proteins[33]. It is possible that the nuclear architecture becomes more susceptible to perturbations at a later age; therefore, the pathological effects of *LMNB1* overexpression may manifest itself only later in adulthood.

Although *LMNB1* was thought to be ubiquitously expressed in all somatic cells, other studies have suggested that it may have a more variable expression pattern[16,34]. It is unclear what the exact levels and patterns of *LMNB1* expression in different regions and cell types of the CNS are. This is crucial for understanding the ADLD duplication phenotype, as cell types that do not express *LMNB1*, or express it at low levels, may be spared the deleterious effects of overexpression. ADLD is characterized by the unique neuropathological findings of preservation of oligodendroglia accompanied by a scarcity of astrocytes[4]. It would be tempting to speculate whether this pathological phenotype was due to the differential susceptibility of astrocytes to *LMNB1* overexpression and whether demyelination is a consequence of this. Demyelination as a result of astrocyte dysfunction has been suggested before for Alexander disease and also in a disease caused by mutations in the gene encoding a protein called MLC1 (refs. 24,35). It is important to note that the levels of overexpression of *LMNB1* in the *D. melanogaster* and cell culture model systems are likely to be greater than those observed in affected individuals. Thus, while the phenotypes we observe in these systems may be more severe than those expected in affected individuals, they would provide useful tools in understanding the disease mechanism.

Although distinct, the clinical phenotype of ADLD shares a number of similarities with chronic progressive multiple sclerosis[4]. Multiple sclerosis is thought to be caused by an autoimmune inflammatory process[36]. Notably, autoantibodies to lamin B have been found in the sera of affected individuals with autoimmune disorders such as systemic lupus erythematosus, scleroderma and autoimmune liver disease[37,38]. Furthermore, the monoclonal antibody J1-31 raised against plaque material from brain tissue of individuals with multiple sclerosis has been shown to recognize lamin B[39]. A recent study has shown that neutrophils that undergo spontaneous apoptosis expressed lamin B1 on the cell surface[40]. As neutrophils are thought to represent an important source of autoantigens in autoinflammatory diseases[40], it provides a further link between lamin B1 and autoimmune diseases. Although the *LMNB1* gene has not been directly implicated in multiple sclerosis, the similarity of clinical phenotypes between ADLD and multiple sclerosis and the identification of autoantibodies to lamin B suggests that a closer examination of the involvement of lamin B1 in multiple sclerosis is warranted.

METHODS

Subjects. The clinical details of the kindreds K2685 and K4975 have been described previously[4,5]. Individuals from K4233 and K50069 were ascertained and clinical analyses carried out similar to analyses in K2685 (ref. 4). DNA was collected from 62 individuals from K2685 and K4233, five individuals from K4975 and three individuals from K50069. Study participants signed a 'Consent

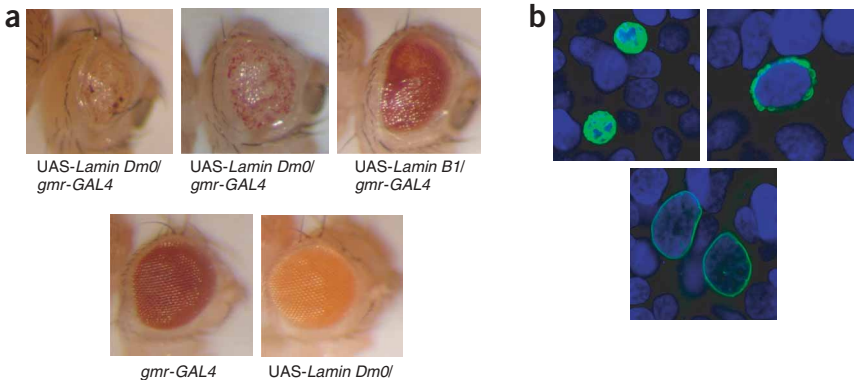

Figure 7 Lamin B1 overexpression in the *D. melanogaster* eye and cell lines. (**a**) Overexpression of the fly *lamin* Dm_0 (upper left and center) and human *LMNB1* (upper right) in the *D. melanogaster* eye using the eye-specific driver *gmr-GAL4*. Eyes of *gmr-GAL4* (lower left) and *UAS-lamin* Dm_0 (lower right) flies. (**b**) Representative micrographs of HEK 293 cells expressing high levels (top row) and low levels (bottom) of LMNB1-GFP with DAPI staining marking the nucleus.

of Participation' form, and procedures were approved by the Institutional Review Board for Human Research at the University of Utah School of Medicine and the University of California at San Francisco. High–molecular weight genomic DNA was isolated from whole-blood lysate using a standard protocol outlined in the Puregene DNA Isolation Kit (Gentra Systems). See **Supplementary Methods** online for details on linkage analysis and hybrid cell line creation.

Gene selection, mutation detection and genotyping. Genes and mRNA sequences in the critical region for the families K2685 and K4233 were identified using successive builds of the UCSC, National Center for Biotechnology Information (NCBI) and Celera genome browsers. Genomic DNA from one affected individual from each of the two families, two controls and one hybrid cell line were analyzed. In all cases, exons for each of the genes, as well as 3′ and 5′ UTR regions and at least 200 bp around the intron-exon boundary, were sequenced. PCR primers were designed using Primer 3 software (http://frodo.wi.mit.edu/cgi-bin/primer3/primer3_www.cgi). PCR was carried out using ~50 ng of genomic DNA and a touch-down protocol[41]. PCR products were purified using Multiscreen PCR purification plates (Millipore), and 50–100 ng was used for sequencing. Sequencing was carried out for both strands using the ABI BigDye Terminator Kit v. 3.1 (Applied Biosystems) according to the manufacturer's instructions. Sequences were analyzed using Sequencher software v. 4.14 (GeneCodes).

We identified new microsatellite markers within the critical region using the simple repeat track in the UCSC genome browser[42]. The two microsatellite markers D5SQ4 and D5SQ12 are both dinucleotide TG repeats. Primers used to amplify these loci are given in **Supplementary Table 3** online. Microsatellite PCR products were fluorescently labeled using a nested PCR protocol described previously[43]. The fluorescently labeled PCR products were then run on a Beckman CEQ 8000 Genetic Analyzer and sizes estimated using the fragment analysis software (Beckman Coulter).

Relative peak height ratio assay. SNP loci from the 'SNP' track of the UCSC genome browser were identified. These loci were typed in samples from affected individuals, and those that were polymorphic in these samples were used for further analysis. PCR for the loci and analysis were carried out as described above. In all cases, relative peak height ratio differences were analyzed in at least two samples from affected individuals and two from controls. Differences between affected individuals and controls were obvious enough to be identified by visual inspection.

DNA blotting. DNA blotting of genomic DNA was used to confirm the duplication in affected individuals from K4233 and K2685. Serial dilutions of 10, 5 and 2.5 μg of DNA from affected individuals and from controls were digested with *Hin*dIII and blotted according to standard protocols[44]. The blot was probed using PCR products that were radioactively labeled using the Prime-It RmT Random Primer labeling Kit (Stratagene) according to the manufacturer's instructions. PCR primers specific for a sequence within the putative duplicated region were used. To check for equal loading, the blot was stripped and reprobed using a probe generated by PCR primers specific for exon 3 of an unrelated gene *SLC30A8* on chromosome 8. The primers used to generate the *LMNB1* and loading control probes are given in **Supplementary Table 3**. Autoradiographs of the blots were scanned and the bands analyzed using the Kodak 1D Image Analysis software v. 3.6. We calculated intensity of the band obtained using the duplication probe and divided it by the intensity of the band obtained using the loading control probe for the same sample and arrived at the value of relative band intensity. We then averaged this relative band intensity value for the three different loading amounts for each sample from affected individuals or controls. This gave us the average relative band intensity, which we plotted in **Figure 3b** for each sample from affected individuals and controls.

TaqMan analysis. TaqMan real-time quantitative PCR analysis was used to quantify both genomic DNA copy number changes and to check for level of expression of *LMNB1* from affected individual and control brain tissue. Primers and probes were designed using Primer Express software (Applied Biosystems). Primers and probes used were specific for exon 4 of the lamin B1 gene and are given in **Supplementary Table 3**. The probe was labeled with a FAM fluorophore as reporter and BHQ-1 as a quencher (Biosearch Technologies). For genomic DNA copy number changes, a probe and primers for the human serum albumin gene were used to normalize sample amounts as described previously[6]. For cDNA expression level analysis, a probe and primers from the GAPDH endogenous control kit (Applied Biosystems) were used to normalize sample amounts. Reactions were carried out on either an ABI 7700 or 7300 real-time PCR machine using the ABI 2× TaqMan universal PCR master mix according to the manufacturer's instructions (Applied Biosystems). For all primer-probe sets used, we confirmed that a doubling of the DNA template amount resulted in a reduction of the threshold cycle number (Ct) by ~1 using serial twofold dilutions of DNA. Samples were run in triplicate, and the mean Ct values were used for calculation. As the different primer-probe sets had similar amplification kinetics, we were able to use the comparative Ct method to detect relative copy number or gene expression as described previously[45]. Using this method, the following formula can be used to calculate the gene copy number or expression relative to a control sample: $2^{-(\Delta\Delta Ct)}$, where $\Delta\Delta Ct$ = [Ct albumin (or GAPDH) (control sample) – Ct lamin B1 (control sample)] – [Ct albumin (or GAPDH) (affected sample) – Ct lamin B1 (affected sample)][6,45].

We used the same *LMNB1* probe and primer sets to measure relative lamin B1 expression. As these primer sets do not cross an intron-exon boundary, they could potentially amplify genomic DNA contamination in the RNA samples used to synthesize cDNA. To exclude this possibility, we also used products from a control reaction without reverse transcriptase (–RT) in the TaqMan reaction. In all cases, the –RT control showed Ct values of at least seven to eight cycles higher than +RT products, suggesting that there was minimal genomic DNA contamination in the cDNA samples.

Long PCR, inverse PCR, duplication junction PCR. Long PCR was carried out using the Expand Long Template PCR system (Roche) according to the manufacturer's instructions. Inverse PCR was carried out to identify the centromeric boundary of the duplication in K2685 and K4233 as described previously[46]. Primers specific for the duplication junctions in K2685 and K4233 were designed and used with the PCR conditions described above.

Bioinformatic analysis of the duplication region and junction sequences. To identify the genes in the putative duplication region and the sequence features around the duplication junction sequences, we used the UCSC genome browser May 2004 assembly (http://www.genome.ucsc.edu). All sequence coordinates used in the paper are based on this assembly. Repetitive elements in the region of the duplication junctions such as short interspersed nucleotide elements (SINEs), long interspersed nucleotide elements (LINEs), long terminal repeats (LTRs) and low-complexity repeats (LCRs) were identified using the repeat masker and simple repeat tracks in the UCSC genome browser[42,47]. Pairwise sequence comparisons of the 2-kb N1-C1 and T2-N2 breakpoint regions for each affected individual were performed using BLAST with default parameters[48] (http://www.ncbi.nlm.nih.gov/BLAST). LCR segments of DNA in a 2-Mb region around the *LMNB1* gene were investigated using PipMaker (http://pipmaker.bx.psu.edu/pipmaker/) with the sequences masked by Repeatmasker, downloaded from the UCSC genome browser[49].

Tissue samples and protein and RNA extraction. Autopsy brain tissue from the cerebral cortex was obtained from three affected members of K2685 and one control subject. The three affected individuals from K2685 were male and died around the age of 60 years. For protein lysates, we homogenized ~100 mg of tissue samples in a DUALL 21 tissue grinder (Kontes) in RIPA lysis buffer (50 mM Tris-HCl pH 7.4, 150 mM NaCl, 1% Triton X-100, 1% sodium deoxycholate, 1% SDS) to which we added Complete Protease Inhibitor Cocktail tablets (Roche). For RNA isolation, tissues were homogenized using a Polytron homogenizer in TRIzol and were extracted according to the manufacturer's protocols (Invitrogen). mRNA was extracted from total RNA using the Oligotex mRNA mini kit (Qiagen). Total brain mRNA from a control individual was also obtained from a commercial source (Ambion).

RNA blotting and RT-PCR analysis. For RNA blotting, we loaded up to 2 μg of mRNA from affected individuals and controls onto a 1.25% precast SeaKem Gold Agarose gel (Cambrex) according to the manufacturer's instructions and performed a blot using standard protocols[44]. A commercially available

multiple–brain tissue RNA blot with RNA from normal controls was also used (Clontech). Blots were probed using PCR products from human brain cDNA that were radioactively labeled as described above. PCR primer sequences for the *LMNB1* probe are given in **Supplementary Table 3**. A β actin probe supplied by the manufacturer (Clontech) was used to normalize RNA amounts and served as an internal loading control. Quantification was carried out as described above for DNA blots.

cDNA was synthesized from mRNA using the Invitrogen SuperScript First Strand Synthesis kit (Invitrogen). mRNA was also used in a mock reverse transcription reaction with all components except the reverse transcriptase enzyme. This '–RT' reaction was used as a control to check for genomic DNA contamination. cDNA was used in the TaqMan quantitative PCR assay using primers described above and in **Supplementary Table 3**. cDNA was also used in standard PCR reactions to check for the presence of various transcripts.

Immunoblot analysis. Protein extracts from tissues from affected individuals and controls in RIPA buffer were separated by SDS-PAGE and transferred to polyvinylidene fluoride (PVDF) membranes according to standard protocols[44]. Blots were incubated in antibodies to lamin B1 (1:500; Zymed) for 1 h at 25 °C. To check for equal loading, blots were stripped and incubated in antibody to α tubulin (1:200,000; Sigma) for 15 min at room temperature. The blot was visualized with horseradish peroxidase–conjugated secondary antibody (Jackson Labs) and enhanced chemiluminescence (Amersham Biosciences). Quantitation was carried out as described above for DNA blots.

Cell culture. HEK293 and HeLa cells were grown under standard conditions and maintained at 37 °C with 5% CO_2. After 1 d, the cells were split into culture slides precoated with poly-L-lysine (Sigma). They were grown to 70–80% confluence and were transfected with 2 μg of pEGFP-*LMNB1* fusion constructs (a gift from J. Ellenberg) using 20 μl of Polyfect reagent (Qiagen). After 1 d, cells were fixed with 4% paraformaldehyde in phosphate buffer for 10 min, rinsed in PBS (pH 7.4) and mounted on Premium microscope slides (Fisher) with Vectashield mounting medium with DAPI (Vector). Images were acquired using a Zeiss Pascal LSM5 confocal microscope in the University of California, San Francisco microscopy core facility and processed with Adobe Photoshop.

***D. melanogaster* genetics.** *SPG-GAL4* and UAS-*lamin* Dm_0 flies were gifts from M. Krasnow and R. Bainton and have been previously described[22,50]. Four lines of the UAS-*lamin* Dm_0 flies were studied. The UAS-*LMNB1* transgenic flies were generated by subcloning the human *LMNB1* cDNA into the region between the *Kpn*I and *Bgl*II sites of the pUAST vector. Plasmids were then injected into *w* embryos to generate transformants, and four independent lines were obtained. All *GAL4* lines were obtained from *D. melanogaster* stock centers. *gmr-GAL4*, *repo-GAL4*, *elav-GAL4* have been described before[19–21].

Note: Supplementary information is available on the Nature Genetics website.

ACKNOWLEDGMENTS

The authors thank the individuals with ADLD and their families for participating in this research. We would like to thank M. Krasnow and R. Bainton for fly stocks and J. Ellenberg for the pEGFP-lamin B1 construct. We are grateful to J. Rawson for fly injections and H.-Y. Lee for confocal microscopy assistance. We thank S. Hauser and J. Oksenberg for discussions. We acknowledge members of the Fu and Ptáček labs for technical assistance and discussions. This work was supported by US National Institutes of Health grant NS41331 (Y.-H.F.), a Sandler Neurogenetics grant (Y.-H.F) and a Pilot grant from the Multiple Sclerosis society (L.J.P.). L.J.P. holds the John C. Coleman Distinguished Professorship in Neurodegenerative Diseases and is an Investigator of the Howard Hughes Medical Institute.

COMPETING INTERESTS STATEMENT

The authors declare that they have no competing financial interests.

Published online at http://www.nature.com/naturegenetics
Reprints and permissions information is available online at http://npg.nature.com/reprintsandpermissions/

1. Schiffmann, R. & van der Knaap, M.S. The latest on leukodystrophies. *Curr. Opin. Neurol.* **17**, 187–192 (2004).
2. Eldridge, R. *et al.* Hereditary adult-onset leukodystrophy simulating chronic progressive multiple sclerosis. *N. Engl. J. Med.* **311**, 948–953 (1984).
3. Schwankhaus, J.D., Katz, D.A., Eldridge, R., Schlesinger, S. & McFarland, H. Clinical and pathological features of an autosomal dominant, adult-onset leukodystrophy simulating chronic progressive multiple sclerosis. *Arch. Neurol.* **51**, 757–766 (1994).
4. Coffeen, C.M. *et al.* Genetic localization of an autosomal dominant leukodystrophy mimicking chronic progressive multiple sclerosis to chromosome 5q31. *Hum. Mol. Genet.* **9**, 787–793 (2000).
5. Asahara, H., Yoshimura, T., Sada, S., Furuya, H. & Kobayashi, T. A Japanese family with probably autosomal dominant adult-onset leukodystrophy. *Rinsho Shinkeigaku.* **36**, 968–972 (1996).
6. Aarskog, N.K. & Vedeler, C.A. Real-time quantitative polymerase chain reaction. A new method that detects both the peripheral myelin protein 22 duplication in Charcot-Marie-Tooth type 1A disease and the peripheral myelin protein 22 deletion in hereditary neuropathy with liability to pressure palsies. *Hum. Genet.* **107**, 494–498 (2000).
7. Inoue, K. *et al.* Genomic rearrangements resulting in PLP1 deletion occur by nonhomologous end joining and cause different dysmyelinating phenotypes in males and females. *Am. J. Hum. Genet.* **71**, 838–853 (2002).
8. Woodward, K.J. *et al.* Heterogeneous duplications in patients with Pelizaeus-Merzbacher disease suggest a mechanism of coupled homologous and nonhomologous recombination. *Am. J. Hum. Genet.* **77**, 966–987 (2005).
9. Richardson, C. & Jasin, M. Coupled homologous and nonhomologous repair of a double-strand break preserves genomic integrity in mammalian cells. *Mol. Cell. Biol.* **20**, 9068–9075 (2000).
10. Super, H.G. *et al.* Identification of complex genomic breakpoint junctions in the t(9;11) MLL-AF9 fusion gene in acute leukemia. *Genes Chromosom. Cancer* **20**, 185–195 (1997).
11. Gillert, E. *et al.* A DNA damage repair mechanism is involved in the origin of chromosomal translocations t(4;11) in primary leukemic cells. *Oncogene* **18**, 4663–4671 (1999).
12. Lupski, J.R. & Stankiewicz, P. Genomic disorders: molecular mechanisms for rearrangements and conveyed phenotypes. *PLoS Genet* **1**, e49 (2005).
13. Inoue, K. PLP1-related inherited dysmyelinating disorders: Pelizaeus-Merzbacher disease and spastic paraplegia type 2. *Neurogenetics* **6**, 1–16 (2005).
14. Stuurman, N., Heins, S. & Aebi, U. Nuclear lamins: their structure, assembly, and interactions. *J. Struct. Biol.* **122**, 42–66 (1998).
15. Lin, F. & Worman, H.J. Structural organization of the human gene (LMNB1) encoding nuclear lamin B1. *Genomics* **27**, 230–236 (1995).
16. Lin, F. & Worman, H.J. Expression of nuclear lamins in human tissues and cancer cell lines and transcription from the promoters of the lamin A/C and B1 genes. *Exp. Cell Res.* **236**, 378–384 (1997).
17. Brand, A.H. & Perrimon, N. Targeted gene expression as a means of altering cell fates and generating dominant phenotypes. *Development* **118**, 401–415 (1993).
18. Bilen, J. & Bonini, N.M. *Drosophila* as a model for human neurodegenerative disease. *Annu. Rev. Genet.* **39**, 153–171 (2005).
19. Ellis, M.C., O'Neill, E.M. & Rubin, G.M. Expression of *Drosophila* glass protein and evidence for negative regulation of its activity in non-neuronal cells by another DNA-binding protein. *Development* **119**, 855–865 (1993).
20. Robinow, S. & White, K. The locus elav of *Drosophila melanogaster* is expressed in neurons at all developmental stages. *Dev. Biol.* **126**, 294–303 (1988).
21. Xiong, W.C., Okano, H., Patel, N.H., Blendy, J.A. & Montell, C. *repo* encodes a glial-specific homeo domain protein required in the *Drosophila* nervous system. *Genes Dev.* **8**, 981–994 (1994).
22. Bainton, R.J. *et al.* moody encodes two GPCRs that regulate cocaine behaviors and blood-brain barrier permeability in *Drosophila*. *Cell* **123**, 145–156 (2005).
23. Favreau, C. *et al.* Expression of lamin A mutated in the carboxyl-terminal tail generates an aberrant nuclear phenotype similar to that observed in cells from patients with Dunnigan-type partial lipodystrophy and Emery-Dreifuss muscular dystrophy. *Exp. Cell Res.* **282**, 14–23 (2003).
24. Mignot, C. *et al.* Alexander disease: putative mechanisms of an astrocytic encephalopathy. *Cell. Mol. Life Sci.* **61**, 369–385 (2004).
25. De Sandre-Giovannoli, A. *et al.* Homozygous defects in LMNA, encoding lamin A/C nuclear-envelope proteins, cause autosomal recessive axonal neuropathy in human (Charcot-Marie-Tooth disorder type 2) and mouse. *Am. J. Hum. Genet.* **70**, 726–736 (2002).
26. Worman, H.J. & Courvalin, J.C. Nuclear envelope, nuclear lamina, and inherited disease. *Int. Rev. Cytol.* **246**, 231–279 (2005).
27. Somech, R., Shaklai, S., Amariglio, N., Rechavi, G. & Simon, A.J. Nuclear envelopathies–raising the nuclear veil. *Pediatr. Res.* **57**, 8R–15R (2005).
28. Bione, S. *et al.* Identification of a novel X-linked gene responsible for Emery-Dreifuss muscular dystrophy. *Nat. Genet.* **8**, 323–327 (1994).
29. Bonne, G. *et al.* Mutations in the gene encoding lamin A/C cause autosomal dominant Emery-Dreifuss muscular dystrophy. *Nat. Genet.* **21**, 285–288 (1999).
30. Hegele, R.A. *et al.* Sequencing of the reannotated *LMNB2* gene reveals novel mutations in patients with acquired partial lipodystrophy. *Am. J. Hum. Genet.* **79**, 383–389 (2006).
31. Lupski, J.R. *et al.* DNA duplication associated with Charcot-Marie-Tooth disease type 1A. *Cell* **66**, 219–232 (1991).
32. Gruenbaum, Y., Margalit, A., Goldman, R.D., Shumaker, D.K. & Wilson, K.L. The nuclear lamina comes of age. *Nat. Rev. Mol. Cell Biol.* **6**, 21–31 (2005).

33. Haithcock, E. *et al.* Age-related changes of nuclear architecture in *Caenorhabditis elegans*. *Proc. Natl. Acad. Sci. USA* **102**, 16690–16695 (2005).
34. Broers, J.L. *et al.* A- and B-type lamins are differentially expressed in normal human tissues. *Histochem. Cell Biol.* **107**, 505–517 (1997).
35. Boor, P.K. *et al.* MLC1: a novel protein in distal astroglial processes. *J. Neuropathol. Exp. Neurol.* **64**, 412–419 (2005).
36. Seboun, E., Oksenberg, J.R. & Hauser, S.L. in *The Molecular and Genetic Basis of Neurological Disease* (eds. Rosenberg, R.N., Prusiner, S.B., DiMauro, S. and Barchi, R.L.) 631–660 (Butterworth-Heinemann, Boston, Massachusetts, 1997).
37. Tan, E.M. Autoantibodies to nuclear lamins. *Ann. Intern. Med.* **108**, 897–898 (1988).
38. Pollard, K.M. *et al. In vitro* posttranslational modification of lamin B cloned from a human T-cell line. *Mol. Cell. Biol.* **10**, 2164–2175 (1990).
39. Garcia, D.M., Weigum, S.E. & Koke, J.R. GFAP and nuclear lamins share an epitope recognized by monoclonal antibody J1-31. *Brain Res.* **976**, 9–21 (2003).
40. Moisan, E. & Girard, D. Cell surface expression of intermediate filament proteins vimentin and lamin B1 in human neutrophil spontaneous apoptosis. *J. Leukoc. Biol.* **79**, 489–498 (2006).
41. Glatt, C.E. *et al.* Screening a large reference sample to identify very low frequency sequence variants: comparisons between two genes. *Nat. Genet.* **27**, 435–438 (2001).
42. Benson, G. Tandem repeats finder: a program to analyze DNA sequences. *Nucleic Acids Res.* **27**, 573–580 (1999).
43. Schuelke, M. An economic method for the fluorescent labeling of PCR fragments. *Nat. Biotechnol.* **18**, 233–234 (2000).
44. Ausubel, F. *et al.* (eds.) *Current Protocols in Molecular Biology.* (John Wiley & Sons, New York, 1999).
45. Livak, K.J. & Schmittgen, T.D. Analysis of relative gene expression data using real-time quantitative PCR and the 2(-delta delta C(T)) method. *Methods* **25**, 402–408 (2001).
46. Triglia, T., Peterson, M.G. & Kemp, D.J. A procedure for *in vitro* amplification of DNA segments that lie outside the boundaries of known sequences. *Nucleic Acids Res.* **16**, 8186 (1988).
47. Smit, A.F. The origin of interspersed repeats in the human genome. *Curr. Opin. Genet. Dev.* **6**, 743–748 (1996).
48. Tatusova, T.A. & Madden, T.L. BLAST 2 Sequences, a new tool for comparing protein and nucleotide sequences. *FEMS Microbiol. Lett.* **174**, 247–250 (1999).
49. Schwartz, S. *et al.* PipMaker–a web server for aligning two genomic DNA sequences. *Genome Res.* **10**, 577–586 (2000).
50. Guillemin, K., Williams, T. & Krasnow, M.A. A nuclear lamin is required for cytoplasmic organization and egg polarity in *Drosophila*. *Nat. Cell Biol.* **3**, 848–851 (2001).

Corrigendum: Lamin B1 duplications cause autosomal dominant leukodystrophy

Quasar S Padiath, Kazumasa Saigoh, Raphael Schiffman, Hideaki Asahara, Takeshi Yamada, Anulf Koeppen, Kirk Hogan, Louis J Ptáček & Ying-Hui Fu

Nature Genetics , doi: 10.1038/ng1872; corrected 12 September 2006

In the version of this article initially published online, the name of one of the authors, Raphael Schiffmann, was misspelled. The error has been corrected for all versions of the article.

Corrigendum: Gain-of-function *SOS1* mutations cause a distinctive form of Noonan syndrome

Marco Tartaglia, Len A Pennacchio, Chen Zhao, Kamlesh K Yadav, Valentina Fodale, Anna Sarkozy, Bhaswati Pandit, Kimihiko Oishi, Simone Martinelli, Wendy Schackwitz, Anna Ustaszewska, Joel Martin, James Bristow, Claudio Carta, Francesca Lepri, Cinzia Neri, Isabella Vasta, Kate Gibson, Cynthia J Curry, Juan Pedro López Siguero, Maria Cristina Digilio, Giuseppe Zampino, Bruno Dallapiccola, Dafna Bar-Sagi & Bruce D Gelb

Nature Genetics; **doi: 10.1038/ng1939; corrected 13 December 2006.**

In the version of this article initially published online, the labels 'expression' in **Figure 2** panels **a**, **b**, and **d** are incorrect. The correct labels are 'activation'. In addition, author Giuseppe Zampino should have affiliation 8 rather than affiliation 7.
These errors have been corrected for all version of the article.

Corrigendum: A recurrent mutation in the BMP type I receptor ACVR1 causes inherited and sporadic fibrodysplasia ossificans progressiva

Eileen M Shore, Meiqi Xu, George J Feldman, David A Fenstermacher, The FOP International Research Consortium, Matthew A Brown & Frederick S Kaplan

Nature Genetics **38, 525–527 (2006); published online 23 April; corrected after print 31 December 2006**

In the version of this article initially published, several contributing authors were listed collectively under the name The FOP International Research Consortium. In order to facilitate the electronic citation of author contributions, the authors have chosen to delete the Consortium name and replace it with the names of the individual consortium authors in alphabetical order. The correct author list and affiliations are as follows:
Eileen M Shore[1–3], Meiqi Xu[1,2], George J Feldman[1,2], David A Fenstermacher[4–6], Tae-Joon Cho[7], In Ho Choi[7], J Michael Connor[8], Patricia Delai[9], David L Glaser[1,2], Martine LeMerrer[10], Rolf Morhart[11], John G Rogers[12], Roger Smith[13], James T Triffitt[14], J Andoni Urtizberea[15], Michael Zasloff[1,2,16,17], Matthew A Brown[14,18] & Frederick S Kaplan[1,2,19]

[1]Center for Research in FOP & Related Disorders, [2]Department of Orthopaedic Surgery, [3]Department of Genetics, [4]Department of Pathology and Laboratory Medicine, [5]Abramson Cancer Center and [6]Biomedical Informatics Facility, University of Pennsylvania School of Medicine, Philadelphia, Pennsylvania 19104, USA. [7]Department of Orthopaedic Surgery, Seoul National University Children's Hospital, Seoul National University College of Medicine, 28 Yeongeon-dong, Jongno-gu, Seoul 110-744, Republic of Korea. [8]Division of Developmental Medicine, Institute of Medical Genetics, University of Glasgow Medical School, Yorkhill Academic Campus, Glasgow G3 8SJ, Scotland, UK. [9]Department of Orthopaedic Surgery, Santa Casa de Misericórdia de São Paulo School of Medicine, Rua Dr. Cesário Motta Jr. 112, Cep: 01221-020, São Paulo, Brazil. [10]Department of Genetics, Hôpital Necker-Enfants Malades, INSERM U-781, 149 Rue de Sèvres, 75015 Paris, France. [11]Department of Pediatrics, Klinikum Garmisch-Partenkirchen GmbH, D-82467 Garmisch-Partenkirchen, Germany. [12]Genetic Health Services Victoria, Department of Genetics, Royal Children's Hospital, Melbourne, Australia. [13]Nuffield Department of Orthopaedic Surgery, Nuffield Orthopaedic Centre, Windmill Road, Headington, Oxford OX3 7LD, UK. [14]Institute of Musculoskeletal Sciences, Botnar Research Centre, Nuffield Orthopaedic Centre, University of Oxford, Oxford OX3 7LD, UK. [15]Assistance Publique - Hôpitaux de Paris (AP-HP), Hôpital Marin, 64700 Hendaye, France. [16]Department of Surgery and [17]Department of Pediatrics, Georgetown University School of Medicine, Washington, DC 20057, USA. [18]Centre for Immunology and Cancer Research, Princess Alexandra Hospital, Ipswich Road, Woolloongabba, Queensland 4102, Australia. [19]Department of Medicine, University of Pennsylvania School of Medicine, Philadelphia, Pennsylvania 19104, USA.

Corrigendum: Lamin B1 duplications cause autosomal dominant leukodystrophy

Quasar S Padiath, Kazumasa Saigoh, Raphael Schiffmann, Hideaki Asahara, Takeshi Yamada, Anulf Koeppen, Kirk Hogan, Louis J Ptáček & Ying-Hui Fu

Nature Genetics **38, 1114–1123 (2006); published online 3 September; corrected online 12 September 2006; corrected after print 22 January 2007**

The construct we described as *moody-GAL4* has a name that was assigned to a different construct in a previously published paper. In this paper, it should be referred to as *SPG-GAL4* (for 'sub-perineural-glia-*GAL4*'). This construct was a gift from R. Bainton (University of California San Francisco School of Medicine). The construction and activity of this promoter will be published elsewhere (R. Bainton, personal communication). The error has been corrected in the PDF version of the article.